Colloid Polym Sci (2010) 288:1233–1243
DOI 10.1007/s00396-010-2252-4

ORIGINAL CONTRIBUTION

Drying dissipative structures of colloidal crystals of silica spheres coated with polymer brushes of poly(carboxymethyl betaine)

Tsuneo Okubo · Hisatomo Suzuki · Hiromi Kitano · Kohji Ohno · Masashi Mizutani · Akira Tsuchida

Received: 18 May 2010 / Accepted: 4 June 2010 / Published online: 23 June 2010

Abstract Drying patterns of colloidal crystals of colloidal silica spheres coated with the brushes of zwitterionic poly (carboxymethyl betaine) (SiP-PCMB) and their parent silica spheres (SiP) were studied on a cover glass, a watch glass, and a Petri glass dish. Crystal structures kept the whole process of dryness of the suspensions of SiP-PCMB and SiP. Crystal structures of the dried films of SiP-PCMB were kept stable even when the initial suspensions contained 5 mM of sodium chloride, which is the important role of the excluded volume effects of the shells of the polymer brushes. On the other hand, crystal structures of SiP spheres in the dried films were much unstable and melted in the presence of 5 mM sodium chloride. In the suspension state, colloidal crystallization of SiP-PCMB took place stably by the contribution of the excluded volume effects besides the extended electrical double layers compared with that of SiP spheres, where only the double layer effect contributes to the crystallization. The fractal patterns of the complexation of SiP-PCMB or SiP spheres with sodium chloride were observed microscopically in the dried films. Several kinds of dissipative crystallization such as array and/or accumulation of the crystallites were observed, and the importance of the convectional and sedimentation processes during the course of dryness was demonstrated.

Keywords Drying dissipative structure · Colloidal crystal · Polymer brush · Poly(carboxymethyl betaine) · Broad ring

Introduction

Most structural patterns in nature form via self-organization accompanied with the *dissipation* of free energy and in the non-equilibrium state. In order to understand the mechanisms of the dissipative self-organization of the simple model systems, instead of the much complex nature itself, the authors have studied the *convectional*, *sedimentary*, and drying dissipative patterns during dryness of colloidal suspensions and solutions as systematically as possible, though these three kinds of structures are strongly correlated and overlap each other [1–3].

Typical *convectional* patterns are Benard cell [4, 5], the *hexagonal circulating* pattern, and *Terada cell* [6–8], the spoke lines spreading the whole liquid surface accompanied with the huge number of cell convections in the normal direction of the spoke lines. These convectional patterns were observed often with the naked eyes in the intermediate and final steps in the convectional processes [9–17]. Recently, the whole processes of the convectional patterns have been clarified experimentally [11, 13, 14]. Theoretical

Electronic supplementary material The online version of this article (doi:10.1007/s00396-010-2252-4) contains supplementary material, which is available to authorized users.

T. Okubo (✉)
Institute for Colloidal Organization,
Hatoyama 3-1-112,
Uji, Kyoto 611-0012, Japan
e-mail: okubotsu@ybb.ne.jp

H. Suzuki · H. Kitano
Department of Applied Chemistry, Graduate School of Science and Engineering, University of Toyama,
Toyama 930-8555, Japan

K. Ohno
Institute for Chemical Research, Kyoto University,
Uji, Kyoto 611-0011, Japan

M. Mizutani · A. Tsuchida
Department of Applied Chemistry, Faculty of Engineering,
Gifu University,
Gifu 501-1193, Japan

studies of the convectional patterns have been reported mainly using Navier–Stokes equations [18–23]. However, these are not always successful when the theories are compared with the experiments.

Sedimentary dissipative patterns during the course of drying suspensions have been studied in detail on a cover glass, a watch glass, a glass dish, and others, for the first time, in our laboratory [11, 24–31]. The broad ring-like patterns were formed in suspension state. It was clarified that the sedimentary particles were suspended above the substrate by the electrical double layers around the particles and always moved by the balancing of the force fields between the convectional flow and the gravitational sedimentation. Quite recently, dynamic bundle-like sedimentary patterns formed cooperatively from the spoke-like convectional structures of coffee [13] and black tea [14] coexisted with cream.

Drying dissipative patterns have been studied for many kinds of colloidal particles [9, 10, 13–17, 24–48], linear-type synthetic and bio-polyelectrolytes [49–51], water-soluble neutral polymers [52, 53], ionic and non-ionic detergents [40, 54, 55], gels [56], colloidal–polymer complex [57], and dyes [58]. The macroscopic broad ring patterns of the hill accumulated with the solutes formed. The broad rings moved inward when solute concentration decreased and/or solute size increased. For the non-spherical particles, the round hill was formed in the central area in addition to the faint broad ring. Macroscopic spoke-like cracks or fine hills including flickering spoke-like ones were also observed for many solutes. Beautiful fractal patterns such as branch-like, arc-like, block-like, star-like, cross-like, and string-like ones were observed in the microscopic scale.

One of the important findings in our experiments is that the primitive vague sedimentary patterns were formed already in the concentrated suspensions or solutions before dryness, and they grew toward fine structures in the processes of the solidification. It has been also clarified that *information* of the suspensions and solutions, shape and size of solute, and atmospheric humidity and temperature, for example, is *transferred* into the drying patterns. Furthermore, *dissipative crystallization* of poly(allylamine hydrochloride) [49], poly(ethylene glycol) [59], sodium salt of poly(methacrylic acid) [60], poly-D-lysine and poly-L-lysine hydrobromides [61], and hydroxypropyl cellulose (Okubo T, Mizutani M, Takahashi S, Tsuchida A, publication in preparation) has been studied in detail. Accumulation, uneven distribution, symmetric distribution and ordering of the polymer single crystals, and further coupling of the single crystals with the dissipative broad ring patterns have been clarified.

In this work, the drying dissipative structures of colloidal crystals of silica spheres attached with the polymer brushes of zwitterionic poly(carboxymethyl betaine) (SiP-PCMB) are studied in detail. Suspensions of the parent colloidal silica spheres and the spheres of polymer brushes showed strong iridescent colors and single crystals. These results support that both the spheres are monodispersed in sphere size. The colloidal particles covered with the polymer brushes are highly interesting to study the role of the electrical double layers around the spheres coated with polymer brushes for the colloidal crystallization, since formation of the double layers are considered to be difficult compared with the solid spheres. Furthermore, the polymer brush spheres are appropriate samples to analyze the relative contributions between the electrical double layers and the excluded volume effect for the soft colloidal crystallization in water. The drying dissipative structures of colloidal crystals have been studied so far for many kinds of colloidal spheres including binary and ternary mixtures and in aqueous and aqueous–alcohol mixtures [10, 15–17, 24–29, 38, 39, 41–46]. It should be mentioned here that the structure, crystallization kinetics, and fundamental properties have been studied in detail by the author's research group [62–65].

Experimental

Materials

Parent colloidal silica spheres (Seahostar KE-P30, SiP) are gifts from Nippon Shokubai Co. Ltd. (Tokyo). The sphere size was 284.0±52.7 nm from dynamic light-scattering (DLS) measurements. The silane coupling reaction of the spheres was made with 3-(2-bromo-2-isobutyryloxy) propyltriethoxysilane (BPE) in ethanol, and the BPE-coated silica spheres (Si-BPE) were obtained (Ohno K, Tsujii Y, publication in preparation). The atomic transfer radical polymerization (ATRP) was further made between Si-BPE and carboxymethylbetaine (CMB) in the presence of ethyl 2-bromoisobutyrate (Et-Br), Cu(I)Br, and 2,2′-bipyridine ([CMB]:[Et-Br]:[CuBr]:[bipyridine]=400:1:8:16) in ethanol (40 ml) at 30 °C for 24 h to give the silica spheres modified with the brushes of SiP-PCMB. It should be noted here that the PCMB brushes prepared by ATRP method have been attached on the gold nanoparticles [66]. A zwitterionic vinyl monomer, 1-carboxy-*N*,*N*-dimethyl-*N*-(2′-methacryloxyoxyethyl)methanaminium inner salt (CMB; commercial name GLBT), was kindly donated by Osaka Organic Chemical Industries, Ltd., Osaka. Chemical structures of CMB monomer and ATRP initiator, BPE, are shown in Scheme 1. The ^{1}H-NMR analysis of an aliquot indicated that the conversion of the polymerization was more than 99%. The unreacted monomer (CMB) and solvent (ethanol) were removed from the suspension of SiP-PCMB by ultrafiltration (Amicon; membrane, Amicon YM-30 (molecular cut-off, 30,000)) with water. Then, the SiP-PCMB was separated from PCMB, which had been

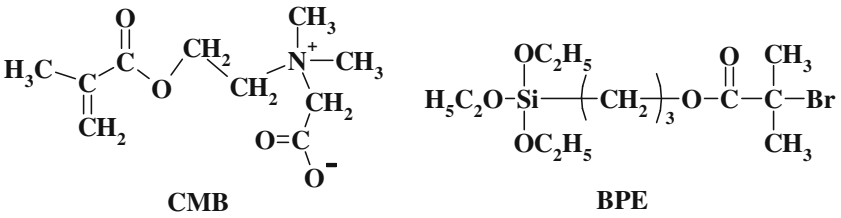

Scheme 1 Chemical structure of CMB and BPE

produced in liquid phase, by ultrafiltration (membrane, Millipore CV (pore size, 0.1 μm)) with water. The aqueous dispersion of SiP-PCMB was slowly passed through a chelate resin column (Amberlite IRC748, Organo, Tokyo) to remove Cu salts and concentrated by further ultrafiltration (membrane, Millipore CV (pore size, 0.1 μm)). The PCMB produced in liquid phase was recovered by the second ultrafiltration described above and, after evaporation of the solvent, was dissolved in water and slowly passed through a chelate resin column to remove Cu salts. The free PCMB was finally lyophilized and characterized by GPC (column, Shodex OHpak SB-803HQ, Showa Denko, Tokyo; mobile phase, 0.1 M NaBr aqueous solution; standard, pullulan, Showa Denko). Sizes of Si-BPE and Si-PCMB were 307± 56.3 and 417±76.6 nm, respectively, from DLS measurements. A shell part of SiP-PCMB sphere was estimated to be composed of ca. 1.1×10^5 of PCMB brushes ($M_n=8.0\times10^4$ estimated by assuming that the M_n value of the PCMB in the brush attached on a SiP core was equal to that produced in the liquid phase [67]). The width of the shell was 66.5 nm, about half of the radius of the core of 142 nm. The zeta-potentials of the SiP-PCMB and SiP spheres were −18.4 and −33.1 mV, respectively, from the electrophoresis light-scattering (ELS) measurements. The water used for the sample preparation was purified by a Milli-Q reagent grade system (Advantage A10, Millipore, Bedford, MA, USA).

Observation of the dissipative structures

Of the colloidal dispersion, 0.1 mL was dropped carefully and gently on a micro-cover glass (30×30 mm, thickness No. 1, from 0.12 to 0.17 mm, Matsunami Glass Co., Kishiwada, Osaka) set in a plastic dish (type NH-52, 52 mm in diameter, 8 mm in depth, As One Co., Tokyo). The cover glasses were used without further rinse. The contact angles for the pure water were 31±0.5° from the drop profiles of water on an unrinsed cover glass. Extrapolation to the zero amount of water was made from measurements at several amounts of water. Of the suspension, 0.7 ml was set on a watch glass (50 mm in diameter, TOP Co., Tokyo). One milliliter was put into a Petri glass dish (27 mm in inner diameter and 15 mm in height, TOP Co.). The disposable serological pipettes (1.0 and 10 ml, codes 7077-1N and 7077-10N, Corning Lab. Sci., Co.) were used for the setting suspensions. Observation of the macroscopic and microscopic patterns was made in a room air-conditioned at 25 °C and 45% to 55% in humidity.

Macroscopic close-up pictures were taken on a Canon EOS 100QD camera with a macro-lens (EF 50 mm, f=2.5) plus a life-size converter EF. Microscopic patterns were observed with a metallurgical microscope (PME-3, Olympus Co., Tokyo). Thickness profiles of the dried films on a cover glass were made on a laser 3D profile microscope (type VK-8500, Keyence Co., Osaka, Japan).

DLS and ELS measurements

The DLS measurements were made on a DLS-7000DL spectrophotometer (Otsuka Electronics, Osaka, Japan) at 25±0.02 °C. The sample of 5 ml was set in a Pyrex tube cell (12 mm in outside diameter and 130 mm long). The zeta-potential measurements were made on an ELS spectrophotometer (LEZA-6000, Otsuka Electronics). The reproducibility of the zeta-potential was within 5%.

Results and discussion

Macroscopic patterns of SiP-PCMB and SiP spheres

Typical examples of the macroscopic patterns during the course of drying suspensions of SiP-PCMB spheres on a cover glass, a watch glass, and a Petri glass dish are shown in Fig. 1a. Initial suspensions emitted weak iridescent colors, since all the suspensions were colloidal crystal state. Appearance of the bluish rings at the drying frontiers and their disappearance were observed with time. Final drying patterns were composed of the whitey broad rings and the bluish in the intermediate regions. Whitey color at the broad ring area is ascribed to the strong multiple scattering of light by the thickly accumulated colloidal crystallites. Note that the drying frontiers started at the outside edge of the initial liquid to the central area on a cover glass and a watch glass. On the other hand, the frontiers moved from the central to outward in a glass dish.

Influence of the initial sphere concentration on the drying patterns of SiP-PCMB is shown in Fig. 1b. On a cover glass, most of the particles were accumulated at the whitey outside

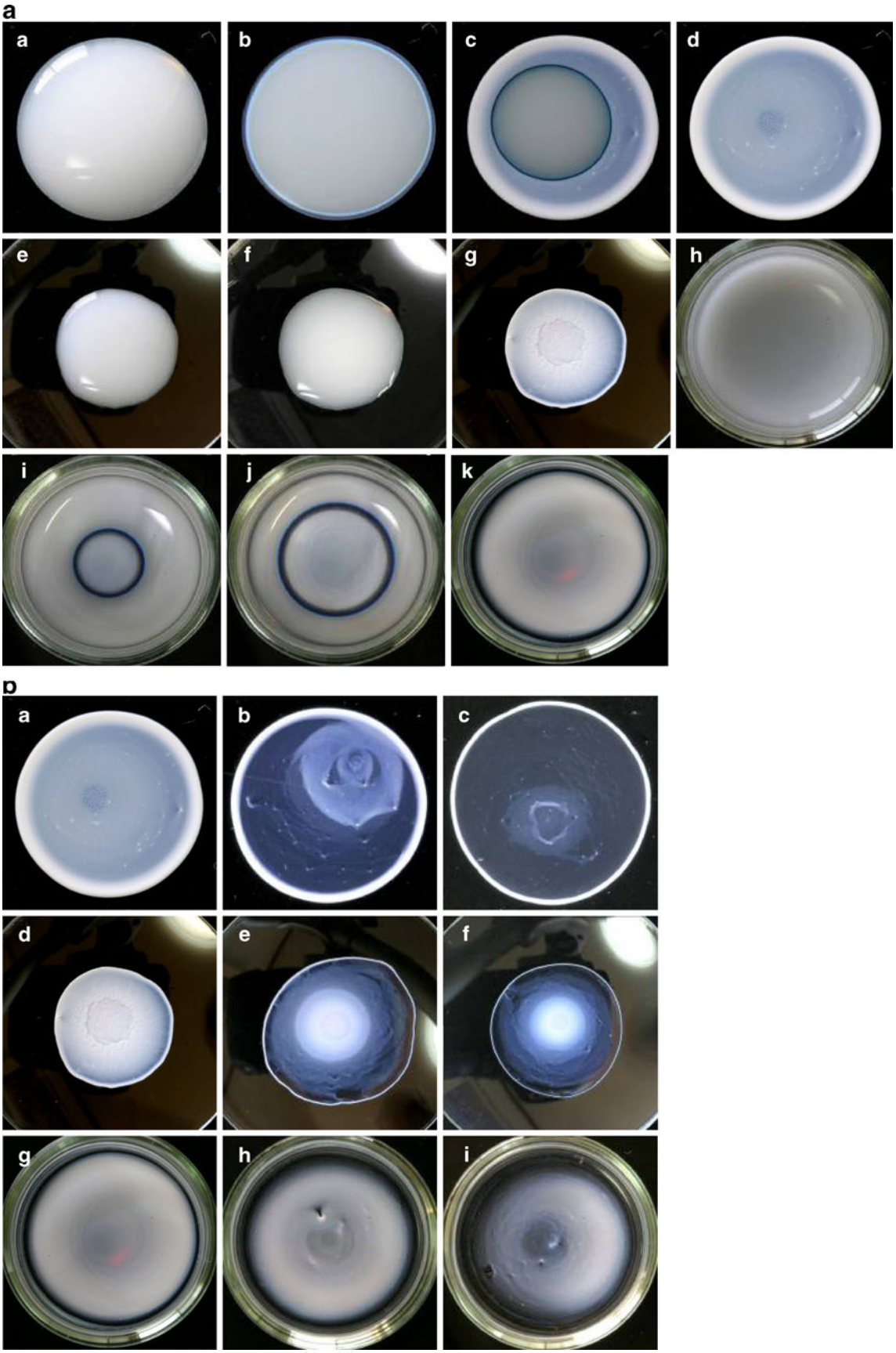
a
a
b
c
d
e
f
g
h
i
j
k
b
a
b
c
d
e
f
g
h
i

◀**Fig. 1** **a** Macroscopic dissipative patterns during dryness of SiP-PCMB on a cover glass (0.1 ml, *a–d*), a watch glass (0.7 ml, *e–g*), and a Petri glass dish (1 ml, *h–k*) at 25 °C. In water, ϕ=0.0174, (*a*) 15 min after setting, (*b*) 2 h 50 min, (*c*) 3 h 45 min; (*d*) 4 h 30 min, (*e*) 20 min, (*f*) 3 h 40 min, (*g*) 16 h 30 min, (*h*) 1 h, (*i*) 9 h 55 min, (*j*) 16 h, (*k*) 29 h 45 min. **b** Macroscopic drying patterns of SiP-PCMB on a cover glass (0.1 ml, *a–c*), a watch glass (0.7 ml, *d–f*), and a Petri glass dish (1 ml, *g–i*) at 25 °C; (*a*, *d*, *g*) ϕ=0.0174, (*b*, *e*, *h*) 0.00522, and (*c*, *f*, *i*) 0.00174

edges forming the broad ring patterns. These broad ring sizes coincided with the initial suspension size. However, the vague broad rings were also recognized at the inner area from the main broad rings, and their size decreased systematically as sphere concentration decreased (see pictures a to c of Fig. 1b). These observations mean that the affinity between SiP-PCMB spheres and the glass substrates is strong enough to keep the drying frontier at the outside edge of the initial suspension drop, and both the colloidal spheres and water molecules continue to flow to the outside edge almost the whole course of the drying process. So many betaine groups of tertiary amines and carboxylic acid moieties of the brushes are highly polar and should interact intimately with the polar silanol groups on the glass wall. It should be noted here that the thinning of the main broad rings was observed with decreasing sphere concentration, as is shown clearly in pictures a to c of Fig. 1b. Thus, it is highly plausible that the broad rings at the outside edges of the initial liquid drop will disappear when the sphere concentration decreases below 0.00174 in volume fraction, where the inner broad rings should come to be the main instead. These changes of the broad rings with the initial sphere concentration have been observed for the suspensions of the colloidal spheres being highly affinitive to the substrate [13, 14]. On a watch glass, the fine broad ring patterns were also observed at the outside edge of the drying films. Furthermore, the broad ring size was almost the same as that of the initial suspension. However, the main broad ring structures appeared at the intermediate region on a watch glass. The ratios of the dried broad ring size against that of the initial suspension decreased as the sphere concentration decreased. This is due to the fact that the inclined cell wall is convenient for the broad ring formation by the convectional flow. In a Petri dish, most of the spheres were now accumulated in the inner region from the cell wall, and their size decreased as sphere concentration decreased. It is interesting to note that the broad ring formation and the concentration dependencies of their size are quite insensitive to the moving directions of the drying frontiers.

Electronic supplementary material Fig. 1 shows the influences of the addition of sodium chloride on the SiP-PCMB dispersions. The drying patterns were insensitive to the salt addition irrespective of the substrates, but the segregation of the low molecular weight salt (NaCl) toward the outside area was recognized in any substrates examined. The influence of the foreign salt was also examined at the initial sphere concentrations of 0.00174 and 0.0174 in volume fraction. Similar observations to Electronic supplementary material Fig. 1 were obtained, though showing the pictures was omitted. Significant segregation effects between the small solutes outward and large ones inward have been observed often in the drying patterns of the colloidal dispersions [16, 25, 28, 29, 31, 46, 51].

Figure 2 shows the drying patterns of the parent colloidal silica spheres SiP on a cover glass (a–c), a watch glass (d–f), and a glass dish (g–i). The drying patterns of SiP spheres were quite similar to those of SiP-PCMB. On a cover glass, at high sphere concentrations, the main broad rings were formed at the outside edge of the initial liquid drops, and they became thin sharply with decreasing sphere concentration. On a watch glass, the broad rings were formed at the intermediate regions, and the rings at the outside edges were quite thin. On a glass dish, most spheres accumulated in the intermediate regions forming broad rings, and their size decreased as the sphere concentration decreased. These observations support that the bare colloidal silica spheres are also quite polar because of their huge number of silanol groups and high affinity with the glass substrates, which have the same silanol moieties on their surfaces. Note here the quite similar drying patterns as Figs. 1b and 2 were observed for the colloidal crystals of colloidal silica [26, 46] and poly(methyl methacrylate) spheres [15–17]. Further study of the salt effects on the SiP dispersions was made. The macroscopic drying patterns were also similar to those of the corresponding SiP-PCMB+NaCl mixtures.

Figure 3 shows the thickness profiles of the dried film of SiP-PCMB at the different sphere concentrations (a–c) and in the presence of sodium chloride (d–f). The main broad rings are clearly located at the outside edges. These profiles do not support the existence of the broad rings in the intermediate regions. However, the flat accumulation of a part of the spheres at the intermediate regions is recognized in Fig. 3a–c. Figure 3d–f shows that the height of the broad ring at the outside edge decreased slightly as the salt concentration increased. The existence of the broad rings in the intermediate regions is supported especially in profiles b and c of the Electronic supplementary material Fig. 2, where the profiles of the parent SiP spheres are shown. Experimental errors were, however, larger than the peak thickness observed. Figure 4 shows the d_f/d_i values as a function of sphere concentration at the various sphere concentrations (open symbols) and in the presence of sodium chloride (solid symbols) on a cover glass (circles), a watch glass (triangles), and a Petri dish (squares). Here, the d_f values are the sizes of the broad rings in the intermediate regions. The d_i values are the sizes of the initial liquid. d_f/d_i values decreased as sphere concentration decreased. However, the differences of d_f/d_i values between SiP-PCMB and SiP spheres did not appear systematically because of the large experimental errors.

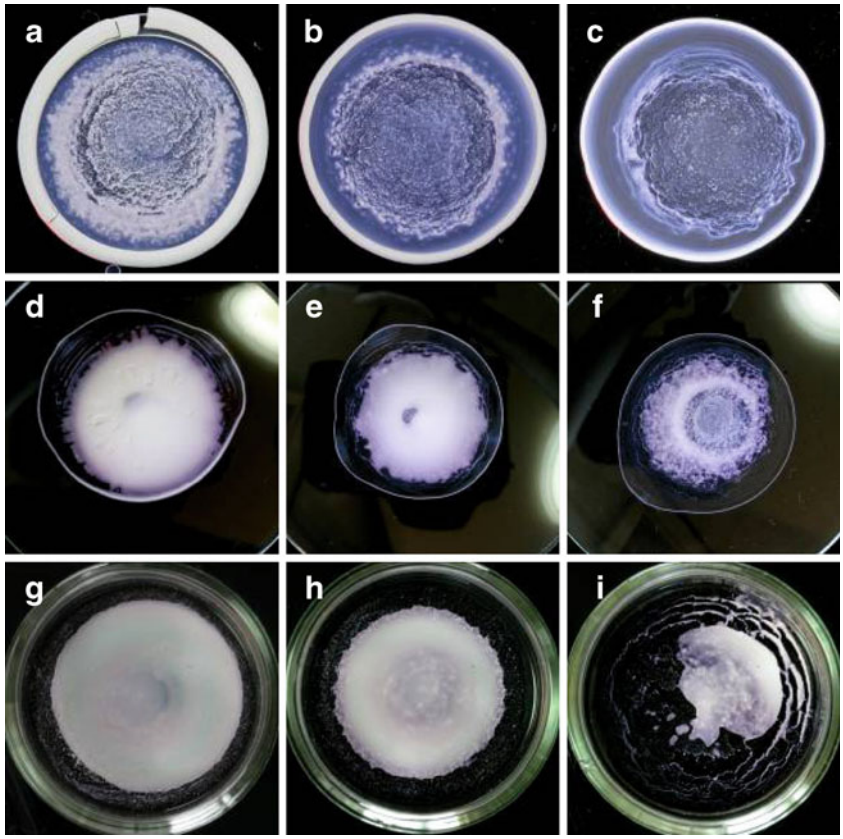

Fig. 2 Macroscopic drying patterns of SiP on a cover glass (0.1 ml, **a**–**c**), a watch glass (0.7 ml, **d**–**f**), and a Petri glass dish (1 ml, **g**–**i**) at 25 °C. **a**, **d**, **g** ϕ=0.0172, (**b**, **e**, **h**) 0.00516, and (**c**, **f**, **i**) 0.00172

Reflection spectroscopy of the dried films of SiP-PCMB and SiP spheres

Figure 5 shows the reflection spectra of the dried films of SiP-PCMB (a–c) from the deionized suspensions (a) and in the presence of sodium chloride (c). The solid, broken, and dotted curves in Fig. 5a show the spectra on a cover glass, a watch glass, and a Petri dish, respectively. On the other hand, the solid, broken, and dotted curves in Fig. 5c are the reflection spectra at [NaCl]=0 M, 0.5 and 5 mM, respectively. Note that the reflection spectra of SiP spheres are also displayed in Fig. 5b, d. The primary peak wavelength

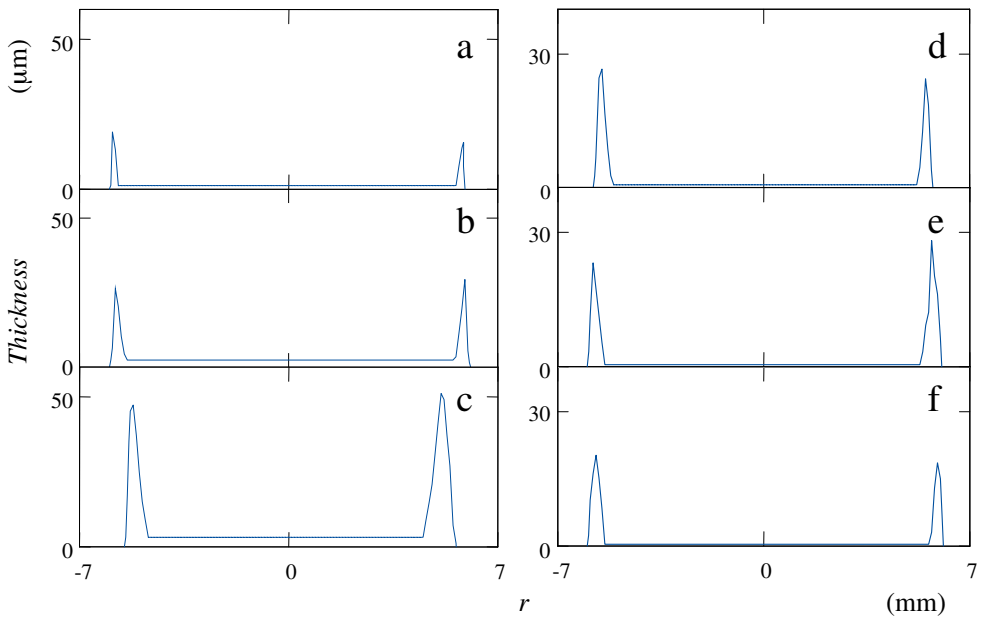

Fig. 3 Thickness profiles of the dried film of SiP-PCMB as a function of the distance from the center on a cover glass at 25 °C. In water, 0.1 ml. **a** ϕ=0.00174, (**b**) 0.00522, (**c**) 0.0174, and (**d**) 0.00522; [NaCl]=0 M, (**e**) 0.00522, 0.0005, (**f**) 0.00522, and 0.005 M

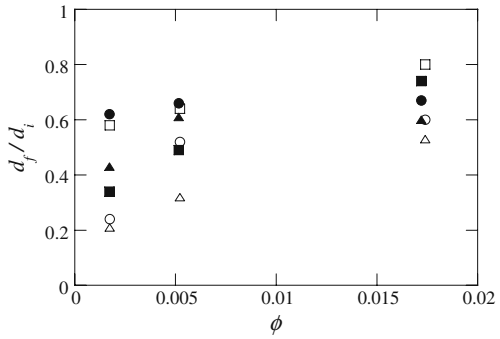

Fig. 4 Plots of d_f/d_i of SiP-PCMB (*open symbols*) and SiP (*closed symbols*) as a function of ϕ on a cover glass (*circles*), a watch glass (*triangles*), and a glass dish (*squares*) at 25 °C

(λp) at the scattering angle of 90° is estimated by Eq. 1 from the nearest-neighbored intersphere distance (l) of the face-centered and/or body-centered cubic lattices.

$$\lambda_p = nl/0.6124 \tag{1}$$

Here, the refractive index of the dried film (n) is given in Eq. 2:

$$n = 0.74 \times [\text{refractive index of SiP} - \text{PCMB(or SiP)}] + 0.26 \times [\text{refractive index of air}] \tag{2}$$

Refractive indices of SiP and air were assumed to be 1.5 and 1.0, respectively. Refractive index of SiP-PCMB sphere was estimated by Eq. 3:

$$[\text{refractive index of SiP} - \text{PCMB}] = ([\text{volume of core}] \times [\text{refractive index of core}] + [\text{volume of shell}] \times [\text{refractive index of shell}])/[\text{volume of SiP} - \text{PCMB}] \tag{3}$$

In order to estimate the refractive index of the shell, the volume ratio of PCMB polymers against shell was calculated first. The excluded sizes of PCMB rod including BPE layer (11.5 nm in width) were assumed to be a rod of 2.6 nm^2 in section area and 66.5 nm in length. Then, the excluded volume of a shell rod is 172.9 nm^3. The total volume of rods in a shell is 1.90×10^7 nm^3 (172.9 $nm^3\times 1.1\times10^5$). Total volume of a shell is calculated to be 2.60×10^7 nm_3 ($\pi4/3$) ($(417/2)^3-(284/2)^3$), which is close to and slightly large compared with the total volume of rods in a shell, 1.90×10^7 nm^3. This agreement supports our appropriate estimation of the excluded volume of a rod. Here, we should note that the real volume of a PCMB chain is estimated roughly to be 4.7 nm^3 ($\pi\times0.15^2\times66.5$ nm), and then the ratio of the real volume against the excluded volume of a rod comes to be 0.027 (4.7/172.9 nm^3). When the refractive index of a PCMB chain is assumed to be 1.5, though the value is not measured yet, the effective refractive index of a PCMB rod is estimated to be 1.01 ($0.027\times1.5+0.973\times1.0$). Thus, the refractive index of the PCMB shell part is assumed soundly to be 1.0. The refractive index of a SiP-PCMB sphere is, therefore, assumed to be 1.16 using Eq. 3. It was further assumed that the addition of sodium chloride did not affect the refractive index of the dried film. The mean λp value of the dried films of SiP-PCMB was 678.5±3 nm in Fig. 5a, c. Thus, the l value is estimated to be 358 nm, which is close to, but small by 14% compared with the diameter of the SiP-PCMB spheres observed by the DLS measurements, 417 nm. When shrinking of the shell in the dried state is taking account, this agreement supports that the SiP-PCMB spheres form crystal distribution keeping contact with the neighboring spheres to each other irrespective of the initial

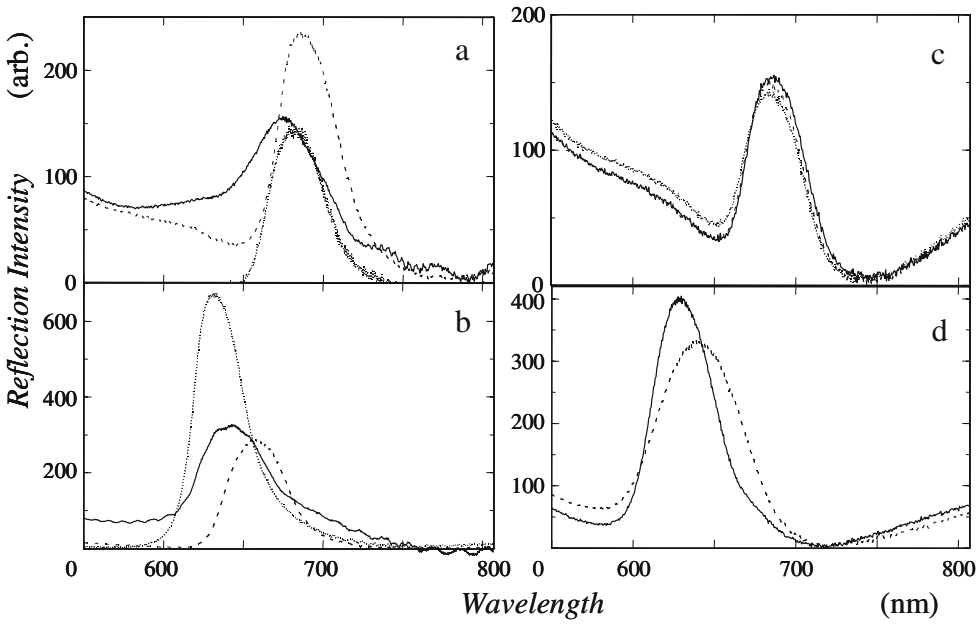

Fig. 5 Reflection spectra of dried film of SiP-PCMB (**a** ϕ= 0.0174, **c** ϕ=0.00522) and SiP (**b** ϕ=0.0172, **d** ϕ=0.00516) at 25 °C. **a**, **b** Deionized suspensions, *solid curve*: on a cover glass, *broken curve*: a watch glass, *dotted curve*: a Petri glass dish. **c**, **d** On a Petri glass dish, *solid curve*: [NaCl]=0 M, *broken curve*: 0.0005 M, *dotted curve*: 0.005 M

concentrations of SiP-PCMB suspensions and also sodium chloride. For the parent SiP spheres, the mean observed λp value of the dried film for the deionized suspensions on a Petri dish shown in dotted curve of b and the solid curve of d was 628±2 nm. The l value thus estimated is 281 nm, which agrees excellently with the diameter of the SiP spheres observed by DLS method, 284 nm. The reflection spectroscopy of the dried film of SiP spheres again supports that the SiP spheres form crystal structure, keeping contact of the spheres to each other. Note here that the peak wavelength on a watch glass in the broken curve in b shifted to longer wavelength. This will be due to the rather large experimental errors in the reflection spectroscopy of the inclined dried films.

It should be mentioned here that the reflection spectra of the dried films of SiP-PCMB are quite similar to each other irrespective of the salt concentration as is shown in spectra c of Fig. 5. On the other hand, the spectra shown in d indicates clearly that the reflection peak of the dried film comes weak, and peak wavelength shifts to longer by the addition of 0.5 mM of sodium chloride. By the addition of 5 mM of NaCl, the reflection peak disappeared, and then the crystalline structures were melted away in the film. These observations indicate that the crystal-like structures in the dried film of SiP-PCMB are quite stable and not destroyed by the salt addition. The colloidal crystallization of SiP-PCMB was not destroyed during the course of solidification by the excluded volume effects of the shell parts of the PCMB brushes. The thickness of the shell and the radius of the core of the parent silica spheres are estimated to be 66.3 and 142 nm as described in the "Experimental" section. Thus, the excluded volume effects of the shell parts on the crystalline structure formation must be significant, i.e., sphere volume of SiP to SiP-PCMB change more than threefold from 1.20×10^7 nm^3 to 3.80×10^7 nm^3 ($(4\pi/3)\times(417/2)^3$). On the other hand, the crystal-like structures of the dried film and also of the initial suspension of SiP spheres are well known to be melted by the addition of sodium chloride, which is clearly ascribed to the sharp thinning of the extended electrical double layers by the addition of sodium chloride. Note that the shift of the spectrum peak toward longer wavelength and even disappearance of the reflection peak in the dried film have been often observed when the colloidal crystals of the initial dispersions are formed only by the extended electrical double layers [24–27, 46].

Microscopic patterns of SiP-PCMB and SiP spheres

Microscopic patterns of SiP-PCMB spheres from the central area to the right edge on a cover glass, a watch glass, and a Petri dish are shown in pictures a–d, c–h, and i–l of Fig. 6, respectively. Iridescent colors are from the Bragg diffraction of light by the crystalline structures of spheres in the dried films. In the pictures, the arrays of the colloidal single crystals along the spoke lines or the ring lines are observed as a function of the distance from the center. The ring-like patterns were observed often especially on a cover glass and the spoke patterns on a watch glass, respectively. In a glass dish, spoke and ring patterns appeared (see Fig. 6j for example).

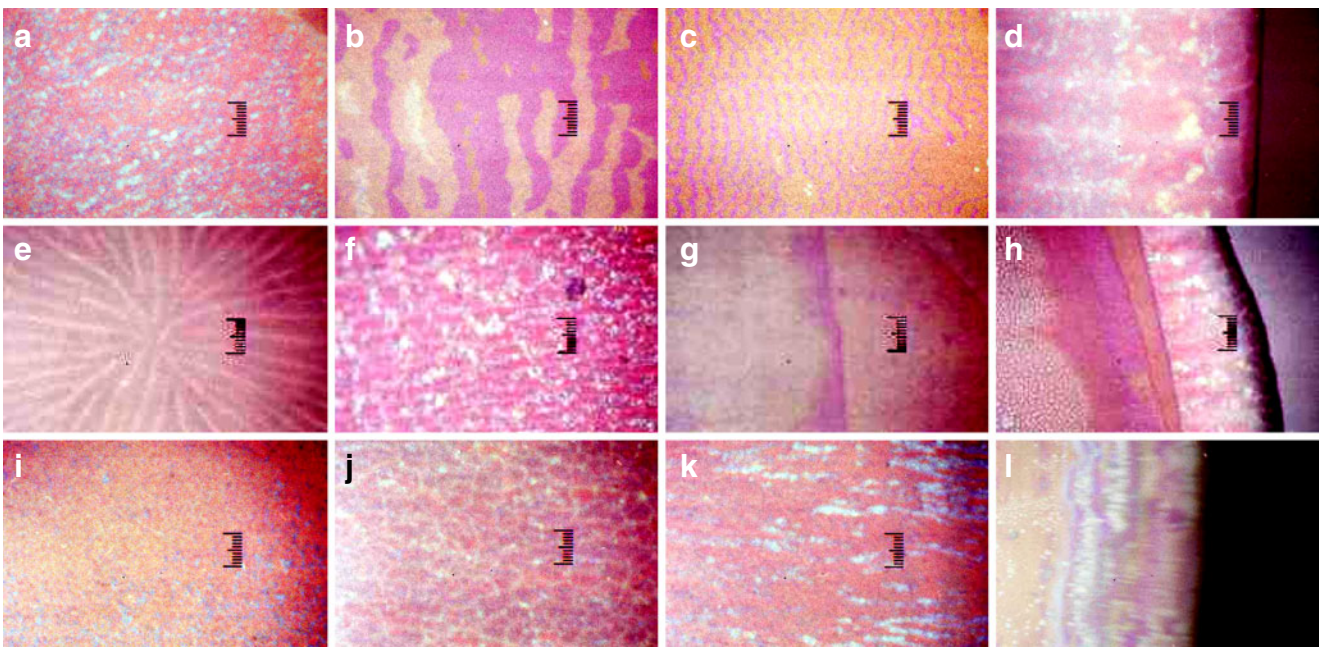

Fig. 6 Microscopic drying patterns of SiP-PCMB on a cover glass (**a**–**d**, 0.1 ml), a watch glass (**e**–**h**, 0.7 ml), and a Petri glass dish (**i**–**l**, 1 ml) at 25 °C. Deionized suspensions, [SiP-PCMB]=0.00522. **a**–**l** The pictures from the center to the right edge, full scale: 50 (**a**–**d**) and 100 μm (**e**–**l**)

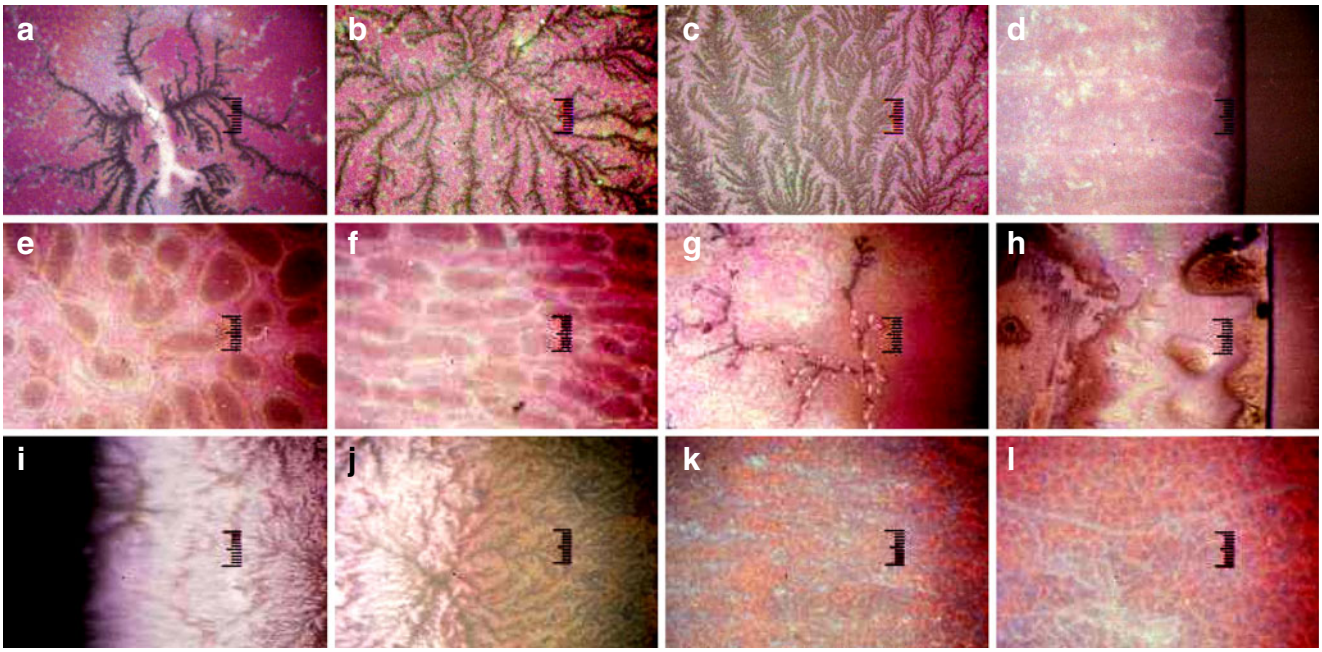

Fig. 7 Microscopic drying patterns of SiP-PCMB on a cover glass (**a**–**d**, 0.1 ml), a watch glass (**e**–**h**, 0.7 ml), and a Petri glass dish (**i**–**l**, 1 ml) at 25 °C. [NaCl]=0.005 M, [SiP-PCMB]=0.00522, **a**–**h** The pictures from the center to the right edge. **i**–**l** From the left edge to the center, full scale: 50 (**a**–**d**) and 100 μm (**e**–**l**)

The microscopic patterns of SiP-PCMB+NaCl systems are shown in Fig. 7 on a cover glass (a–d), a watch glass (e–h), and a Petri glass dish (i–l), respectively. The cooperated and fractal patterns of SiP-PCMB spheres with sodium chloride appeared in Fig. 7a–c. Here, black dendritic structures are composed of the colloidal spheres. Note that these fractal structures have been observed for the mixtures of colloidal silica spheres and sodium chloride [25].

Typical microscopic patterns of SiP spheres are shown in Fig. 8 on a cover glass (a–d), a watch glass (e–h), and a Petri glass dish (i–l), respectively. Sharp color bands especially in the outside area were observed on a cover glass and a watch glass. Furthermore, the radial directed

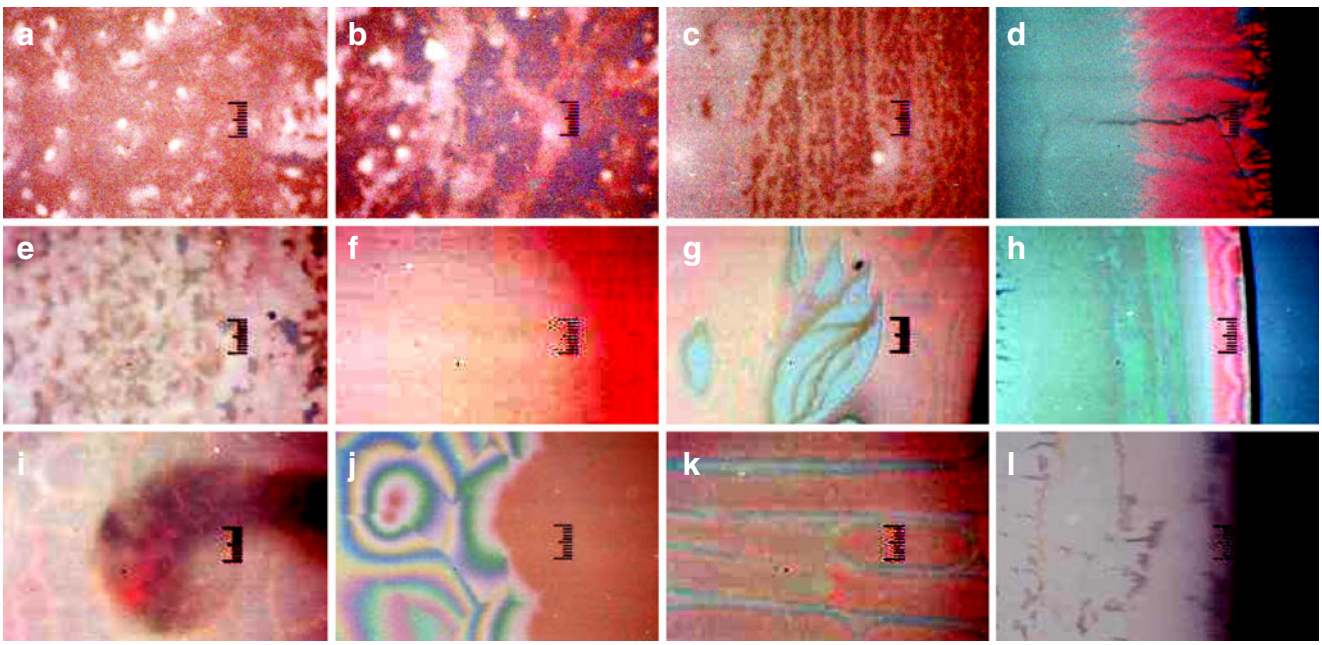

Fig. 8 Microscopic drying patterns of SiP on a cover glass (**a**–**d**, 0.1 ml), a watch glass (**e**–**h**, 0.7 ml), and a Petri glass dish (**i**–**l**, 1 ml) at 25 °C. Deionized suspensions, [SiP]=0.00516. **a**–**l** The pictures from the center to the right edge, full scale: 50 (**a**–**d**) and 100 μm (**e**–**l**)

(spoke-like) and ring-like orientation of the colloidal single crystals was observed as a function of the distance from the center of the dried film on all the substrates examined. Note that these microscopic pictures resemble those of the colloidal crystals studied so far [24–27, 46].

Concluding remarks

The stable crystal-like structures of SiP-PCMB spheres are formed both in suspension and the dried film states by the important contribution of the excluded volume effects of the shell parts of the spheres. Furthermore, the zeta-potential of the dispersion of SiP-PCMB spheres was negative, which is the same as the most colloidal crystal systems in aqueous dispersion state. It should be recalled here that the stable colloidal crystallization in aqueous dispersion took place for several kinds of core-shell type colloidal spheres [68, 69]. The colloidal crystallization of the polymer modified colloidal silica spheres with the shells of polystyrene, poly(methyl methacrylate), and poly(styrene-co-maleic anhydride) took place in the various polar organic solvents mainly by the extended electrical double layers [70, 71]. The main cause of the small contribution of the excluded volume effects on the colloidal crystallization will be due to the less dense polymer shells compared with the SiP-PCMB spheres in the present work.

Several kinds of dissipative colloidal crystallization such as array and/or broad ring-like accumulation of the crystallites were observed. Morphologies of colloidal crystals in the dried film have been influenced greatly by the successive and dissipative processes of convection, sedimentation, and solidification during dryness. Among the many processes, the convectional flow steps will be most important for the orientation of the single crystals in the dried film. The spoke-like flow shown by Benard cell [4, 5] and Terada cell [6–8] and the large number of cell convections of the Terada cell must be the main origin for the radial and ring-like orientations of the single crystals in the suspension state, respectively. It should be mentioned here that the morphologies of polymer crystals were also influenced strongly by the dissipative processes of convection, sedimentation, and solidification. Conformational information of poly(allylamine hydrochloride) in the initial aqueous solution was transferred to the microscopic drying patterns of crystals [49]. Symmetrical ordering of the polymer single crystals and further coupling of the spherulites and the lamellae originated from the broad ring patterns were observed during dryness of aqueous solution of poly(ethylene glycol) [59] and sodium salt of poly(methacrylic acid) [60]. Shape and size of the single crystals of polylysine changed greatly as a function of the distance from the center of the drying film [61].

Acknowledgments Financial supports from the Ministry of Education, Culture, Sports, Science, and Technology, Japan, and Japan Society for the Promotion of Science are greatly acknowledged for Grants-in-Aid for Exploratory Research and Scientific Research (B), respectively. The authors are grateful to Osaka Organic Chemical Industries, Ltd., for the gift of CMB monomer. Nippon Shokubai Co., Tokyo, and REX Co., Tokyo, are thanked deeply for providing the colloidal silica sphere samples used in this work and research grants, respectively.

References

1. Okubo T (2006) In: Stoylov SP, Stoimenova MV (eds) Molecular and colloidal electro-optics. Taylor & Francis, New York, p 573
2. Okubo T (2008) In: Nagarajan R, Hatton TA (eds) Nanoparticles: syntheses, stabilization, passivation and functionalization. ACS Book, Washington DC, p 256
3. Okubo T (2010) Macromol Symp 288:67
4. Gribbin G (1999) Almost everyone's guide to science. The universe, life and everything. Yale University Press, New Haven
5. Ball P (1999) The self-made tapestry. Pattern formation in nature. Oxford Univ Press, Oxford
6. Terada T, Yamamoto R, Watanabe T (1934) Sci Pap Inst Phys Chem Res Jpn 27:173, Proc Imper Acad Tokyo 10:10
7. Terada T, Yamamoto R, Watanabe T (1934) Sci Pap Inst Phys Chem Res Jpn 27:75
8. Nakaya U (1947) Memoirs of Torahiko Terada (Japanese). Kobunsya, Tokyo
9. Okubo T, Kimura H, Kimura T, Hayakawa F, Shibata T, Kimura K (2005) Colloid Polym Sci 283:1
10. Okubo T (2006) Colloid Polym Sci 285:225
11. Okubo T (2009) Colloid Polym Sci 287:167
12. Deegan RD, Bakajin O, Dupont TF, Huber G, Nagel SR, Witten TA (1997) Nature 389:827
13. Okubo T, Okamoto J, Tsuchida A (2009) Colloid Polym Sci 287:351
14. Okubo T (2009) Colloid Polym Sci 287:645
15. Okubo T, Okamoto J, Tsuchida A (2008) Colloid Polym Sci 286:1123
16. Okubo T (2008) Colloid Polym Sci 286:1307
17. Okubo T (2008) Colloid Polym Sci 286:1527
18. Palmer HJ (1976) J Fluid Mech 75:487
19. Anderson DM, Davis SH (1995) Phys Fluids 7:248
20. Pouth AF, Russel WB (1998) AIChEJ 44:2088
21. Burelbach JP, Bankoff SG (1998) J Fluid Mech 195:463
22. Deegan RD, Bakajin O, Dupont TF, Huber G, Nagel SR, Witten TA (2000) Phys Rev E 62:756
23. Fischer BJ (2002) Langmuir 18:60
24. Okubo T (2006) Colloid Polym Sci 284:1191
25. Okubo T (2006) Colloid Polym Sci 284:1395
26. Okubo T, Okamoto J, Tsuchida A (2007) Colloid Polym Sci 285:967
27. Okubo T (2007) Colloid Polym Sci 285:1495
28. Okubo T, Okamoto J, Tsuchida A (2008) Colloid Polym Sci 286:385
29. Okubo T, Okamoto J, Tsuchida A (2008) Colloid Polym Sci 286:941
30. Yamaguchi T, Kimura K, Tsuchida A, Okubo T, Matsumoto M (2005) Colloid Polym Sci 283:1123
31. Okubo T (2006) Colloid Polym Sci 285:331
32. Vanderhoff JW (1973) J Polym Sci Symp 41:155
33. Nicolis G, Prigogine I (1977) Self-organization in non-equilibrium systems. Wiley, New York
34. Ohara PC, Heath JR, Gelbart WM (1997) Angew Chem 109:1120
35. Maenosono S, Dushkin CD, Saita S, Yamaguchi Y (1999) Langmuir 15:957

36. Nikoobakht B, Wang ZL, El-Sayed MA (2000) J Phys Chem 104:8635
37. Ung T, Litz-Marzan LM, Mulvaney P (2001) J Phys Chem B 105:3441
38. Okubo T, Okuda S, Kimura H (2002) Colloid Polym Sci 280:454
39. Okubo T, Kimura K, Kimura H (2002) Colloid Polym Sci 280:1001
40. Okubo T, Kanayama S, Kimura K (2004) Colloid Polym Sci 282:486
41. Okubo T, Yamada T, Kimura K, Tsuchida A (2005) Colloid Polym Sci 283:1007
42. Okubo T, Nozawa M, Tsuchida A (2007) Colloid Polym Sci 285:827
43. Okubo T, Kimura K, Tsuchida A (2007) Colloids Surf B Biointerfaces 56:201
44. Okubo T, Nakagawa N, Tsuchida A (2007) Colloid Polym Sci 285:1247
45. Okubo T, Kimura K, Tsuchida A (2008) Colloid Polym Sci 286:621
46. Okubo T (2008) Colloid Polym Sci 286:1411
47. Okubo T, Otake A, Tsuchida A (2009) Colloid Polym Sci 287:1435
48. Okubo T, Kokufuta E, Nakamuro M, Yoshinaga K, Mizutani M, Tsuchida A (2010) Colloids Surfaces B Biopolym. doi:10.1016/jcolsurb.2010.06.004
49. Okubo T, Kanayama S, Ogawa H, Hibino M, Kimura K (2004) Colloid Polym Sci 282:230
50. Okubo T, Onoshima D, Tsuchida A (2007) Colloid Polym Sci 285:999
51. Okubo T, Ogawa H, Tsuchida A (2010) Colloid Polym Sci 288:245
52. Shimomura M, Sawadaishi T (2001) Curr Opin Colloid Interface Sci 6:11
53. Okubo T, Yamada T, Kimura K, Tsuchida A (2006) Colloid Polym Sci 284:396
54. Kimura K, Kanayama S, Tsuchida A, Okubo T (2005) Colloid Polym Sci 283:898
55. Okubo T, Shinoda C, Kimura K, Tsuchida A (2005) Langmuir 21:9889
56. Okubo T, Itoh Emi, Tsuchida A, Kokufuta E (2006) Colloid Polym Sci 285:339
57. Okubo T, Okamoto J, Tsuchida A (2010) Colloid Polym Sci 288:189
58. Okubo T, Yokota N, Tsuchida A (2007) Colloid Polym Sci 285:1257
59. Okubo T, Okamoto J, Takahashi S, Tsuchida A (2009) Colloid Polym Sci 287:933
60. Okubo T, Hagiwara A, Kitano H, Okamoto J, Takahashi S, Tsuchida A (2009) Colloid Polym Sci 287:1155
61. Okubo T, Okamoto J, Tsuchida A (2010) Colloid Polym Sci 288:981
62. Okubo T (1988) Acc Chem Res 21:281
63. Okubo T (1993) Prog Polym Sci 18:481
64. Okubo T, Tsuchida A (2002) Forma 17:141
65. Okubo T (2008) Polym J 40:882
66. Matsuura K, Ohno K, Kagaya S, Kitano H (2007) Macromol Chem Phys 208:862
67. Ohno K, Morinaga T, Koh K, Tsujii Y, Fukuda T (2005) Macromolecules 38:2137
68. Okubo T, Kimura H, Hase H, Lovell PA, Erington N, Thong P (2005) Colloid Polym Sci 283:393
69. Okamoto J, Kimura H, Tsuchida A, Okubo T, Ito K (2007) Colloids Surf B Biointerfaces 56:231
70. Okubo T, Ishiki H, Chiyoda M, Yoshinaga K (2002) Colloid Polym Sci 280:290
71. Yoshinaga K, Chiyoda M, Ishiki H, Okubo T (2002) Colloids Surfaces A 204:285